Time–Evolving Statistics of Chaotic Orbits of Conservative Maps in the Context of the Central Limit Theorem

G. Ruiz,[1] T. Bountis,[2] and C. Tsallis[3,4]

[1]*Departamento de Matemática Aplicada y Estadística, Universidad Politécnica de Madrid, Pza. Cardenal Cisneros s/n, 28040 Madrid, Spain*

[2]*Department of Mathematics and Center for Research and Applications of Nonlinear Systems (CRANS) and University of Patras, GR26500, Rion, Patras (Greece)*

[3]*Centro Brasileiro de Pesquisas Fisicas and National Institute of Science and Technology for Complex Systems, Rua Xavier Sigaud 150, 22290-180 Rio de Janeiro, Brazil*

[4]*Santa Fe Institute, 1399 Hyde Park Road, Santa Fe, New Mexico 87501, USA*

(Dated: October 12, 2010)

Abstract

We study chaotic orbits in conservative low–dimensional maps and present numerical results showing that the probability density functions (pdfs) of the sum of N iterates in the $N \to \infty$ limit exhibit very interesting time-evolving statistics, in the sense of the Central Limit Theorem. In some cases where the chaotic layers are thin and the (positive) maximal Lyapunov exponent small, long–lasting quasi–stationary states (QSS) are found, whose pdfs appear to converge to q–Gaussians associated with nonextensive statistical mechanics. More generally, however, as N increases, the pdfs describe a sequence of QSS that pass from a q–Gaussian to a triangular shape and ultimately tend to a true Gaussian, as orbits diffuse to larger chaotic domains, where Lyapunov exponents attain larger values and the phase space dynamics approaches uniform ergodicity.

I. INTRODUCTION

As is well–known, invariant closed curves of area–preserving maps present complete barriers to orbits moving inside resonance islands in the two–dimensional phase space. Outside these regions, there exist families of smaller islands and invariant Cantor sets (often called cantori), to which chaotic orbits are observed to "stick" for very long times. Thus, at the boundaries of these islands, an 'edge of chaos' develops with vanishing Lyapunov exponents, where trajectories yield quasi-stationary states (QSS) that are often very long–lived. In this paper we study numerically, in the sense of the Central Limit Theorem (CLT), probability density functions (pdfs) of such QSS, aiming to understand the connection between their intricate phase space dynamics and their time–evolving statistics.

One such connection is already known to exist: When the dynamics is bounded and uniformly hyperbolic (as e.g. in the case of Sinai billiards) the associated pdf is a Gaussian. However, even in nonhyperbolic conservative models, there are regions where trajectories are essentially ergodic and mixing, so that Gaussians are ultimately observed in the classical CLT sense, as the number of iterations grows. In such cases the maximal Lyapunov exponent is positive and bounded away from zero. What happens, however, when the motion is "weakly" chaotic and explores domains with intricate invariant sets, where the maximal (positive) Lyapunov exponent is very small? It is the purpose of this work to explore the statistics of such regions and determine the type of QSS generated by their dynamics.

Recently, there has been a number of interesting studies of pdfs of one–dimensional maps [**?** **?** **?**] and many examples of higher–dimensional conservative maps [**?** **?** **?** **?** **?**] in precisely such 'edge of chaos' domains, where the maximal Lyapunov exponent either vanishes or is very close to zero. This suggests the convenience for a more thorough investigation of these systems within a nonextensive statistical mechanics approach, based on the nonadditive entropy S_q [**?** **?**]. According to this approach, the pdfs optimizing (under appropriate constraints) S_q are q–Gaussian distributions of sums of variables and represent metastable states [**?** **?**], or QSS of the dynamics. Even for deterministic systems, the validity of a CLT has been verified [**?** **?**] and, more recently, a q-generalization of the CLT was proved demonstrating that, for certain classes of strongly correlated random variables, their rescaled sum approaches a q-Gaussian limit distribution [**?** **?**].

In this paper, we follow this reasoning and compute first, in such weakly chaotic domains

of conservative maps, the pdf of the rescaled sum of N iterates in the $N \to \infty$ limit and for many different initial conditions. We then connect our results with specific properties of the phase space dynamics of the maps and distinguish cases where the pdfs represent long–lived QSS described by q–Gaussians. We generally find that, as N grows, these pdfs pass from a q–Gaussian to a triangular shape, ultimately tending to become true Gaussians, as "stickiness" to cantori apparently subsides in favor of more uniformly chaotic (or ergodic) motion.

In section II we begin our study by a detailed study of QSS and their pdfs and corresponding dynamics in two–dimensional Ikeda and MacMillan maps. In section III we briefly discuss analogous phenomena in 4–dimensional conservative maps and end with our conclusions in section IV.

II. TWO–DIMENSIONAL AREA–PRESERVING MAPS

Let us consider two–dimensional maps of the form:

$$\begin{cases} x_{n+1} = f(x_n, y_n) \\ y_{n+1} = g(x_n, y_n) \end{cases} \tag{1}$$

and treat their chaotic orbits as generators of random variables. Even though this is not true for the iterates of a single orbit, we may still regard as random sequences those produced by many independently chosen initial conditions. In [**?**], the well known CLT assumption about the independence of N identically distributed random variables was replaced by a weaker property that essentially means asymptotic statistical independence. Thus, we may proceed to compute the generalized rescaled sums of their iterates x_i in the classical CLT spirit:

$$Z_N = N^{-\gamma} \sum_{i=1}^{N} (x_i - \langle x \rangle) \tag{2}$$

For fully chaotic systems ($\gamma = 1/2$), the distribution of (**??**) in the limit ($N \to \infty$) is expected to be a Gaussian [**? ? ?**]. Alternatively, however, we may define the non–rescaled variable z_N

$$z_N = \sum_{i=1}^{N} [x_i - \langle x \rangle] \tag{3}$$

and analyze the pdf of z_N normalized by its variance (so as to absorb the rescaling factor N^γ) as follows:

First, we construct the sums $S_N^{(j)}$ obtained from the addition of N x-iterates x_i ($i = 0, \ldots, N$) of the map (**??**)

$$S_N^{(j)} = \sum_{i=0}^{N} x_i^{(j)} \tag{4}$$

where (j) represents the dependence of $S_N^{(j)}$ on the randomly chosen initial conditions $x_0^{(j)}$, with $j = 1, 2, ..., N_{ic}$. Next, we focus on the centered and rescaled sums

$$s_N^{(j)} \equiv \left(S_N^{(j)} - \langle S_N^{(j)} \rangle\right) / \sigma_N = \left(\sum_{i=0}^{N} x_i^{(j)} - \frac{1}{N_{ic}} \sum_{j=1}^{N_{ic}} \sum_{i=0}^{N} x_i^{(j)}\right) / \sigma_N \tag{5}$$

where σ_N is the standard deviation of the $S_N^{(j)}$

$$\sigma_N^2 = \frac{1}{N_{ic}} \sum_{j=1}^{N_{ic}} \left(S_N^{(j)} - \langle S_N^{(j)} \rangle\right)^2 = \langle {S_N^{(j)}}^2 \rangle - \langle S_N^{(j)} \rangle^2 \tag{6}$$

Plotting the histograms of $P(s_N^{(j)})$, we look for the limit distributions as $N \to \infty$, and check if they are well fitted by a q-Gaussian:

$$P(s_N^{(j)}) = P(0) \left(1 + \beta(q-1)(s_N^{(j)})^2\right)^{\frac{1}{1-q}} \tag{7}$$

where q is the index of the nonadditive entropy S_q and β is a 'inverse temperature' parameter. Note that as $q \to 1$ this distribution tends to a Gaussian, i.e., $\lim_{q\to 1} P(s_N^{(j)}) = P(0) e^{-\beta (s_N^{(j)})^2}$. For now on, we write $z/\sigma \equiv s_N^{(j)}$.

A. The Ikeda map

Let us first examine by this approach the well–known Ikeda map [**?**]

$$\begin{cases} x_{n+1} = R + u(x_n \cos\tau - y_n \sin\tau) \\ y_{n+1} = u(x_n \sin\tau + y_n \cos\tau) \end{cases} \tag{8}$$

where $\tau = C_1 - C_2/(1 + x_n^2 + y_n^2)$, where R, u, C_1, C_2 are free parameters, and the Jacobian is $J(R, u, \tau) = u^2$, so that (**??**) is dissipative for $u < 1$ and area-preserving for $u = 1$. This map was proposed as a model, under some simplifying assumptions, of the type of cell that might be used in an optical computer. Fixing the values of $C_1 = 0.4$, $C_2 = 6$ and $R = 1$

we observe in Figure **??** different structures of the phase space dynamics for representative values of the parameter, u.

The values of the positive (largest) Lyapunov exponent L_{max} in these cases are listed in the Table **??** below.

u	0.7	0.8	0.9	1.0
L_{max}	0.334	0.344	0.5076	0.118

TABLE I: Maximal Lyapunov exponents of the Ikeda map, with $C_1 = 0.4$, $C_2 = 6$, $R = 1$ and $u = 0.7, 0.8, 0.9, 1.0$.

Figure **??** shows the corresponding pdf of the normalized variables (**??**) obtained for some typical values of the parameter u, in the limit ($N \to \infty$). We observe that for $u < 1$, the system possesses strange chaotic attractors, whose pdfs can be properly fitted by Gaussians. These numerical results are not in disagreement with those of [**?**], who analyzed the 2–dimensional Hénon map and showed that its strange attractor exhibits nonextensive properties (i.e., $q \neq 1$). In a fully chaotic domain, non-extensive properties need not be present and consequently pdfs of the sum of iterates should be Gaussian distributions. Now, for $u = 0.7, 0.8, 0.9$, the Ikeda map (**??**) generates strange attractors whose maximum Lyapunov exponent is positive and bounded away from zero (see Table **??**). This means that the motion is *not* at the 'edge of chaos' but rather in a chaotic sea and consequently the concepts involved in Boltzmann-Gibbs statistics are expected to hold. On the contrary, for the area-preserving case $u = 1$, the pdf of the sums of (**??**) converges to a non-Gaussian function (see Fig. **??**: $u = 1$).

Now, in an 'edge of chaos' regime, one might expect to obtain a q-Gaussian limit distribution ($q < 3$), as they are a generalization of Gaussians and extremize the nonadditive entropy S_q [**?**] under appropriate constraints. Of course, the chaotic annulus shown in the 3d panel of Fig. **??** for $u = 1$ does not represent an 'edge of chaos' regime, as the maximal Lyapunov exponent does not vanish (see Table **??**) and the orbit appears to explore this annulus more or less uniformly. Hence a q-Gaussian distribution in that case would not be expected. But appearances can be deceiving. The result we obtain is remarkable, as the

central part of our pdf is well–fitted by a q-Gaussian functional with $q = 5.3$ up to very large N (see 4th panel of Fig. **??**). Although this is not a normalizable q-Gaussian function (since $q > 3$ [**?**]), it is nevertheless striking enough to suggest that: (a) the motion within the annular region is not as uniformly ergodic as one might have expected and (b) the L_{max} is not large enough to completely preclude 'edge of chaos' dynamics.

All this motivated us to investigate carefully similar phenomena in another family of area-preserving maps.

B. The MacMillan map

Consider the so–called perturbed MacMillan map, which may be interpreted as describing the effect of a simple linear focusing system supplemented by a periodic sequence of thin nonlinear lenses [**?**]:

$$\begin{cases} x_{n+1} = y_n \\ y_{n+1} = -x_n + 2\mu \frac{y_n}{1+y_n^2} + \epsilon \left(y_n + \beta x_n \right) \end{cases} \tag{9}$$

where ϵ, β, μ are physically important parameters. The Jacobian is $J(\epsilon, \beta) = 1 - \epsilon\beta$, so that (**??**) is area-preserving for $\epsilon\beta = 0$, and dissipative for $\epsilon\beta > 0$. Here, we only consider the area-preserving case $\beta = 0$, so that the only relevant parameters are (ϵ, μ).

The unperturbed map yields a lemniscate invariant curve with a self-intersection at the origin that is a fixed point of saddle type. For $\epsilon \neq 0$, separatrices split and the map presents a thin chaotic layer around two islands. Increasing ϵ, chaotic region spreads.

Within these chaotic regions, we have analyzed the histogram of the normalized sums of (**??**) for a wide range of parameters (ϵ, μ) and have identified some generic pdfs in the form of *q-Gaussians*, and *stretched exponentials* $\sim e^{-k|z|}$ having a triangular shape on semi-logarithmic scale, which we call for convenience *triangular distributions*. Monitoring their 'time evolution' under increasingly large numbers of iterations N, we typically observe the occurrence of different QSS described by these distributions. We have also computed their L_{max} and corresponding phase space plots and summarized our main results in Figures **??** and **??**.

Below, we discuss the time-evolving statistical behavior of two examples of the Mac Millan map, which represent respectively: (1) One set of cases with a 'figure eight' chaotic

region which passes through a succession of pfds before converging to an ordinary Gaussian (Figure 3), and (2) a set with more complicated chaotic domains extending around many islands, where q-Gaussian pdfs dominate the statistics for very long times and convergence to a Gaussian is not observed (Figure 4).

1. ($\epsilon = 0.9$, $\mu = 1.6$)–MacMillan map

The (0.9, 1.6)–MacMillan map is a typical example producing time–evolving pdfs. As shown in Figure **??**, the corresponding phase space plots yield a seemingly simple chaotic region in the form of a 'figure eight' around two islands, yet the corresponding pdfs do *not converge* to a single distribution; rather they pass from a q-Gaussian to a *triangular* distribution.

Analyzing carefully this time evolution of pdfs, we observed that there exist at least three long–lived QSS, whose iterates mix in the 2–dimensional phase space to generate superimposed pdfs of the corresponding sums (**??**). Consequently, for $i = 1 \dots N = 2^{16}$, a QSS is produced whose pdf is close to a pure ($q = 1.6$)–Gaussian whose β parameter increases as the density of phase space plot grows, i.e., increasing N (see Figure **??**). This kind of distribution, in a fully chaotic region, is not only due to a Lyapunov exponent quite close to zero, but also to a "stickiness" effect around islands of regular motion. In fact, the boundaries of these islands is where the 'edge of chaos' regime is expected for conservative maps [**?**]. The maximal Lyapunov exponents for the cases shown in Figures **??** and **??** are listed in Table **??** below.

ϵ	0.2	0.5	0.9	1.1	1.2	1.8
L_{max}	0.0867	0.082	0.0875	0.03446	0.0513	0.05876

TABLE II: Maximal Lyapunov exponents of the MacMillan map, with $\mu = 0.6$ and $\epsilon = 0.2, 0.5, 0.9, 1.1, 1.2, 1.8$.

Figure **??** and Figure **??** show some phase space plots for a number of iterates N. Note that for $N = 1 \dots 2^{16}$, these plots depict at first a 'figure eight' chaotic region that evolves essentially around two islands. For $N > 2^{16}$, however, a more complex structure emerges: Iterates stick around new islands, and an alternation of QSS is evident from q-Gaussian to exponentially decaying shapes (see Figure **??**).

Clearly, therefore, in the case of $\epsilon = 0.9$, more than one QSS coexist whose pdfs are the superposition of their corresponding $(q \neq 1)$–Gaussians. In fact, note in Figure **??** that this superposition of QSS occurs for $10^{18} \leq N \leq 2^{21}$ and produces a mixed distribution where central part is still well–described by a $(q = 1.6)$–Gaussian. However, as we continue to iterate the map to $N = 2^{23}$, this q–Gaussian is hidden by a superposition of intermediate states, passing to a *triangular* distribution. From here on, as $N > 2^{23}$, the central part of the pdfs is close to a Gaussian (see Fig. **??** and Fig. **??**) and a true Gaussian is expected in the limit $(N \to \infty)$. The evolution of this sequence of successive QSS as N increases is shown in detail in Fig. **??**.

2. ($\epsilon = 1.2$, $\mu = 1.6$)–MacMillan map

Let us now carefully analyze the behavior of the $\epsilon = 1.2$ ($\mu = 1.6$) case of the MacMillan map, whose maximum Lyapunov exponent is $L_{max} \approx 0.05$, smaller than that of the $\epsilon = 0.9$ case ($L_{max} \approx 0.08$, see Figure **??**). As is clearly seen in Figure **??**, a diffusive behavior sets in here that extends outward in phase space, spreading finally around the islands of an order 8 resonance to which the orbits "stick" as the number of iterations grows to $N = 2^{19}$.

Again, chaotic motion starts by enveloping the same 'figure eight' as in the $\epsilon = 0.9$ case and the central part of the corresponding pdf attains a $(q = 1.6)$-*Gaussian* form for $N \leq 2^{16}$ (see left panel of Fig. **??**). No transition to a different QSS is detected, until the orbits diffuse to a wider chaotic region in phase space, for $N \leq 2^{18}$. Let us observe in Figure **??** the corresponding pdfs of the rescaled sums of iterates, where even the tail of the pdf appears to converge to a $(q = 1.6)$-Gaussian (right panel of Fig. **??**). For larger N, further diffusion ceases as orbits "stick" to the outer islands, where the motion stays from there on. This only affects the tail of the distribution, which now further converges to a true $(q = 1.6)$-*Gaussian* representing this QSS up to $N = 2^{20}$).

The remaining cases of Figures **??** and **??** can be viewed from a similar perspective. Indeed, the above analysis of the $\epsilon = 1.2$ example can serve as a guide for the $(\epsilon = 0.5, \mu = 1.6)$– and $(\epsilon = 1.1, \mu = 1.6)$–MacMillan maps, as well. In every case, the smallness of the L_{max} but also the details of the diffusion process seem to play a key role in explaining the convergence of pdfs to a q-Gaussian. What differs is the particular phase space picture that emerges and the number of iterations required to achieve the corresponding QSS.

Let us finally examine more carefully our results on the MacMillan map for $\mu = 1.6$ and $\epsilon = 0.2, 0.9, 1.8$, which share a rather simple dynamics around the two islands of the 'figure eight' chaotic region. Their associated pdfs seem to pass rather quickly from a q-Gaussian shape to exponential to Gaussian. By contrast, the cases with $\epsilon = 0.5, 1.1, 1.2$ possess a chaotic domain that is considerably more convoluted around many more islands and hence apparently richer in "stickiness" phenomena. This higher complexity of the dynamics may very well be the reason why these latter examples have QSS with q–Gaussian-like distributions that persist for very long. Even though we are not at an 'edge of chaos' regime where $L_{max} = 0$, it appears that it is the detailed structure of chaotic regions, with their network of islands and invariant sets of cantori, which is responsible for obtaining QSS with long-lived q-Gaussian distributions in conservative systems.

III. FOUR–DIMENSIONAL CONSERVATIVE MAPS

We now briefly discuss some preliminary results on the occurrence of QSS and nonextensive statistics in a 4–dimensional symplectic mapping model of accelerator dynamics [**?**]. This model describes the effects of sextupole nonlinearities on a hadron beam passing through a cell composed of a dipole and two quadrupole magnets, which focuses the particles' motion in the horizontal (x)– and vertical (y)–directions [**?**]. After some appropriate scaling, the equations of the mapping are written as follows:

$$\begin{cases} x_{n+1} = 2c_x x_n - x_{n-1} - \rho x_n^2 + y_n^2 \\ y_{n+1} = 2c_y y_n - y_{n-1} + 2x_n y_n \end{cases} \tag{10}$$

where $\rho = \beta_x s_x / \beta_y s_y$, $c_{x,y} \equiv \cos(2\pi q_{x,y})$ and $s_{x,y} \equiv \sin(2\pi q_{x,y})$, $q_{x,y}$ is the so-called betatron frequencies and $\beta_{x,y}$ are the betatron functions of the accelerator. As in [**?**], we assume that $\beta_{x,y}$ are constant and equal to their mean values, i.e. proportional to $q_{x,y}^{-1}$ ($q_x = 0.21$, $q_y = 0.24$) and place our initial conditions at a particular point in 4-dimensional space associated with weak diffusion phenomena in the y–direction. In particular, our $(x_0, x_1) = (-0.0049, -0.5329)$ coordinates are located within a thin chaotic layer surrounding the islands around a 5-order resonance in the x_n, x_{n-1} plane of a purely horizontal beam, i.e. when $y_n = y_{n-1} = 0$. We then place our initial y_1, y_0 coordinates very close to zero and observe the evolution of the y_ns indicating the growth of the beam in the vertical direction

as the number of iterations N increases.

Let us observe this evolution in Figure **??** separately in the x_{n+1}, x_n and y_{n+1}, y_n 2–dimensional projections of our chaotic orbits. Clearly the behavior of these projections is very different: In the x–plane the motion keeps evolving in a thin chaotic layer around five islands, "feeding" as it were the (y_n, y_{n+1}) oscillations, which show an evidently slow, diffusive growth of their amplitude outward.

In Table **??** we list, for different initial values of y_0 ($y_1 = 0$), the maximum amplitude of the y–oscilaltions, y_{max}, while Figure **??** shows the corresponding pdfs of the normalized sums of iterates of the y_n-variable. Note that, just as in the case of 2–dimensional maps, these distributions are initially *q-Gaussian*-like evolving slowly into *triangular*-like distributions, which finally approach Gaussians. In Figure **??** we follow this evolution by performing four computations of $N = 2^{19}$ iterates starting with y_0 which increases every time by a factor of 10.

case	y_0	y_{max}
1	0.00001	0.00002
2	0.0001	0.0003
3	0.001	0.004
4	0.01	0.015

This similarity with the 2–dimensional case makes us suspect that the orbits of our 4–dimensional map also follow a sequence of weakly chaotic QSS, whose time–evolving features are depicted in plots of the y–motion in Fig **??**, for increasing N. Note, for example, that one such QSS is apparent up to $N = 2^{19}$, when its amplitude is suddenly tripled in the y–direction. The pdf of this QSS is shown in the upper left panel of Fig **??** and has the shape of a q–Gaussian up to this value of N. However, due to the sudden increase of the y_n amplitudes at $N = 2^{20}$, the "legs" of the pdf are lifted upward and the distribution assumes a more triangular shape.

This rise of the pdf "legs" to a triangular shape is shown in more detail in Figure **??**, for initial conditions $y_0 = 10^{-5}, 10^{-4}$, as the number of iterations grows to $N = 2^{20}$. Clearly, the *closer we start* to $y_0 = y_1 = 0$ the more our pdf resembles a q–Gaussian, while as we move further out in the y_0–direction our pdfs tend more quickly towards a Gaussian–like shape. This sequence of distributions is reminiscent of what we found for the 2–dimensional MacMillan map at $(\epsilon = 0.9, \mu = 1.6)$. Recall that, in that case also, a steady slow diffusion

was observed radially outward, similar to what was observed for the 4–dimensional map (**??**), which does not appear to be limited by a closed invariant curve in the x_n, y_n plane.

One might wonder if it is possible to obtain for the 4-dimensional map (**??**) also long–lived q–Gaussian pdfs of the type we found in the 2–dimensional MacMillan map. The likelihood of this occurrence is small, however, as all orbits we computed for the accelerator map (**??**) eventually *escaped to infinity*! This implies that stickiness phenomena on island boundaries and sets of cantori are more dominant and tend to slow down diffusion in the plane of the MacMllan map much more than in the 4–dimensional space of the accelerator map. It would, therefore, be very interesting to study, in a future paper, higher–dimensional maps whose chaotic orbits *never escape* to infinity (e.g. coupled standard maps) and compare their statistics with what we have discovered for the examples treated in the present paper.

IV. CONCLUSIONS

Our work serves to connect different types of statistical distributions of chaotic orbits (in the spirit of the Central Limit Theorem) with different aspects of the dynamics in the phase space of conservative systems. What we have found, in several examples of the McMillan and Ikeda 2–dimensional area preserving maps as well as one case of a 4–dimensional symplectic accelerator map, is that q-Gaussians represent quasi-stationary states (QSS), which are surprisingly long–lived, especially when the orbits evolve in a complicated chaotic region surrounding many islands. This may be attributed to the fact that the maximal Lyapunov exponent in these regions is small and the dynamics occurs close to the so–called "edge of chaos" where stickiness effects are important near the boundaries of these islands.

On the other hand, in simpler–looking chaotic domains (surrounding e.g. only two major islands) the observed QSS passes, as time evolves, from a q–Gaussian to a *triangularly* shaped pdf and may in fact become Gaussian, as the number of iterations becomes arbitrarily large. Even in these cases, however, the successive QSS are particularly long-lasting, so that the Gaussians expected from uniformly ergodic motion are practically unobservable.

Interestingly enough, similar results have been obtained in N-dimensional Hamiltonian systems [**?** **?**] describing FPU particle chains near nonlinear normal modes which have just turned unstable as the total energy is increased. Since these models evolve in a multi–dimensional phase space, the q–Gaussian pdfs last for times typically of the order 10^6, then

pass quickly through the triangular stage and converge to Gaussians, as chaotic orbits move away from thin layers to wider "seas", where Lyapunov exponents are much larger. However, as long as the motion evolves near an "edge of chaos" region the distributions are q-shaped for long times, exactly as we found in the present paper.

These conclusions are closely related to results obtained by other authors [**?** **?**], who also study QSS occurring in low-dimensional Hamiltonian systems like 2-D and 4-D maps, but not from the viewpoint of sum distributions. They define a variance of momentum distributions they call "temperature" $T(t)$ and show numerically that it follows a "sigmoid" curve starting from small values and converging to a final value, which they identify as the Boltzmann Gibbs (BG) state. Although their initial conditions are spread over a wide domain and do not start from a precise location in phase space as we do, they also discover many examples of QSS which remain at the initial temperature for very long times, before finally converging to the BG state.

Acknowledgments

We acknowledge partial financial support by CNPq, Capes and Faperj (Brazilian Agencies) and DGU-MEC (Spanish Ministry of Education) through Project PHB2007-0095-PC. One of us (T. B.) is grateful for the hospitality of the Centro Brasileiro de Pesquisas Fisicas, at Rio de Janeiro, during March 1 – April 5, 2010, where part of the work reported here was carried out.

---

[1] U. Tirnakli, C. Beck and C. Tsallis, Phys. Rev. E **75**, 040106(R) (2007).

[2] U. Tirnakli, C. Tsallis and C. Beck, Phys. Rev. E **79**, 056209 (2009).

[3] O. Afsar and U. Tirnakli, Phys. Rev. E **82**, 046210 (2010).

[4] F. Baldovin, E. Brigatti and C. Tsallis, Phys. Lett. A **320**, 254 (2004).

[5] F. Baldovin, L. G. Moyano, A. P. Majtey, A. Robledo and C. Tsallis, Physica A **340**, 205 (2004).

[6] G. Casati, C. Tsallis and F. Baldovin, Eurohys. Lett. A **72**, 355 (2005).

[7] S.M.Duarte Queiros, Phys. Let. A **373**, 1514 (2009).

[8] L. G. Moyano, A. P. Majtey and C. Tsallis, Eur. Phys. J. B**52**, 493 (2006).

[9] C. Tsallis, J. Stat. Phys. **52**, 479 (1988).

[10] C. Tsallis, Introduction to Nonextensive Statistical Mechanics - Approaching a Complex World (Springer, New York, 2010).

[11] G. Miritello, A. Pluchino and A.Rapisarda, Physica A **388**, 4818 (2009).

[12] A. Rodríguez, V. Schwammle and C. Tsallis, J. Stat. Mech. P09006 (2008).

[13] C. Beck and G. Roepstorff, Physica A **145**, 1 (1987); C. Beck, J. Stat. Phys. **79**, 875 (1995).

[14] M.C.Mackey and M. Tyran-Kaminska, Phys. Rep. **422**, 167 (2006).

[15] S. Umarov, C. Tsallis and S. Steinberg, Milan J. of Math. **76**, 307 (2008); see also S. Umarov, C. Tsallis, M. Gell-Mann and S. Steinberg, J. Math. Phys. **51**, 033502 (2010).

[16] M. G. Hahn, Xi. Jiang and S. Umarov, J. Phys. A: Math. Teor. **43** (16), 165208 (2010).

[17] Z. Galias, Nonlinearity **15**, 1759 (2002).

[18] U. Tirnakli, Phys. Rev. E **66**, 066212 (2002).

[19] C. Beck, Phys. Rev. Lett. **87**, n. 18, 180601 (2001).

[20] V. Papageorgiou, L. Glasser and T. Bountis, J. Appl. Math. **49** (3), 692 (1989).

[21] G. M. Zaslavskii , R. Z. Sagdeev, D. A. Usikov and A. A. Chernikov, *Weak Chaos and Quasi-Regular Patterns*, Cambridge Nonlinear Science Series **1** (Cambridge University Press, Cambridge, 1991).

[22] T. Bountis, and St. Tompaidis, in *Nonlinear Problems in Future Particle Accelerators*, W. Scandale and G. Turchetti, eds. (World Scientific, Singapore, 1991) p.112.

[23] T. Bountis and M. Kollmann, Phys. D **71**, 122 (1994).

[24] C. Antonopoulos, T. Bountis and V. Basios, *Quasi–Stationary Chaotic States in Multi–Dimensional Hamiltonian Systems*, submitted for publication (2010). http://arxiv.org/abs/1009.3049

[25] M. Leo, R.A. Leo and P. Tempesta, *J. Stat. Mech.: Th. & Exp.* **04**, P04021 (2010).

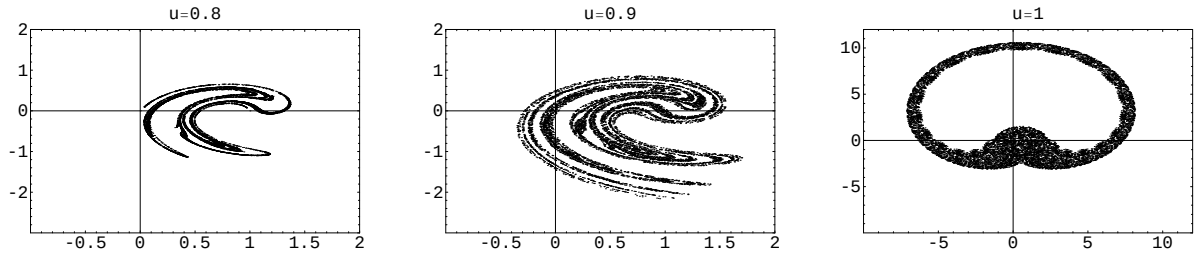

FIG. 1: Phase space plots of the Ikeda map for $C_1 = 0.4$, $C_2 = 6$, $R = 1$, and representative values of u. When $u = 0.8, 0.9, \cdots < 1$, areas of the phase plane contract and strange attractors appear. When $u = 1$, the map is area–preserving and a chaotic annular region is observed surrounding a domain about the origin, where the motion is predominantly quasiperiodic. We use randomly chosen initial conditions from a square $[0, 10^{-4}] \times [0, 10^{-4}]$.

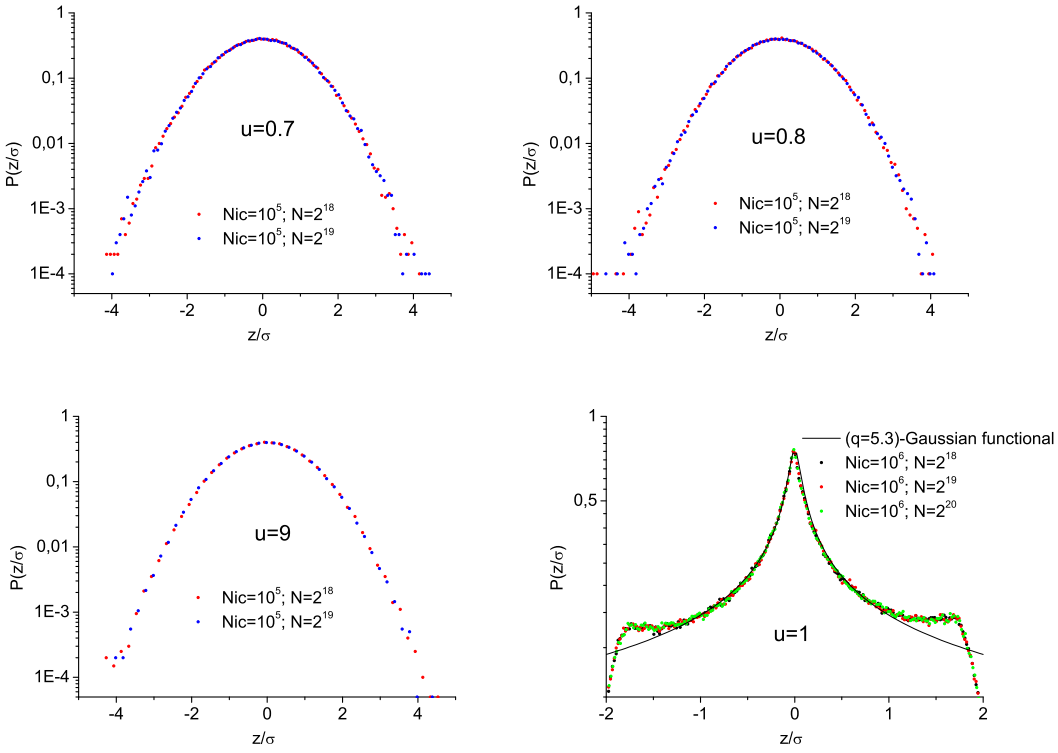

FIG. 2: Pdfs of the normalized sums of iterates of the Ikeda map, for $C_1 = 0.4$, $C_2 = 6$, $R = 1$ and $u = 0.7, 0.8, 0.9, 1.0$. N represents the number of (summed) iterates, N_{ic} is the number of randomly chosen initial conditions from the basin of attraction of the dissipative cases and a square $[0, 1] \times [0, 1]$ located inside the chaotic annular region of the area-preserving map.

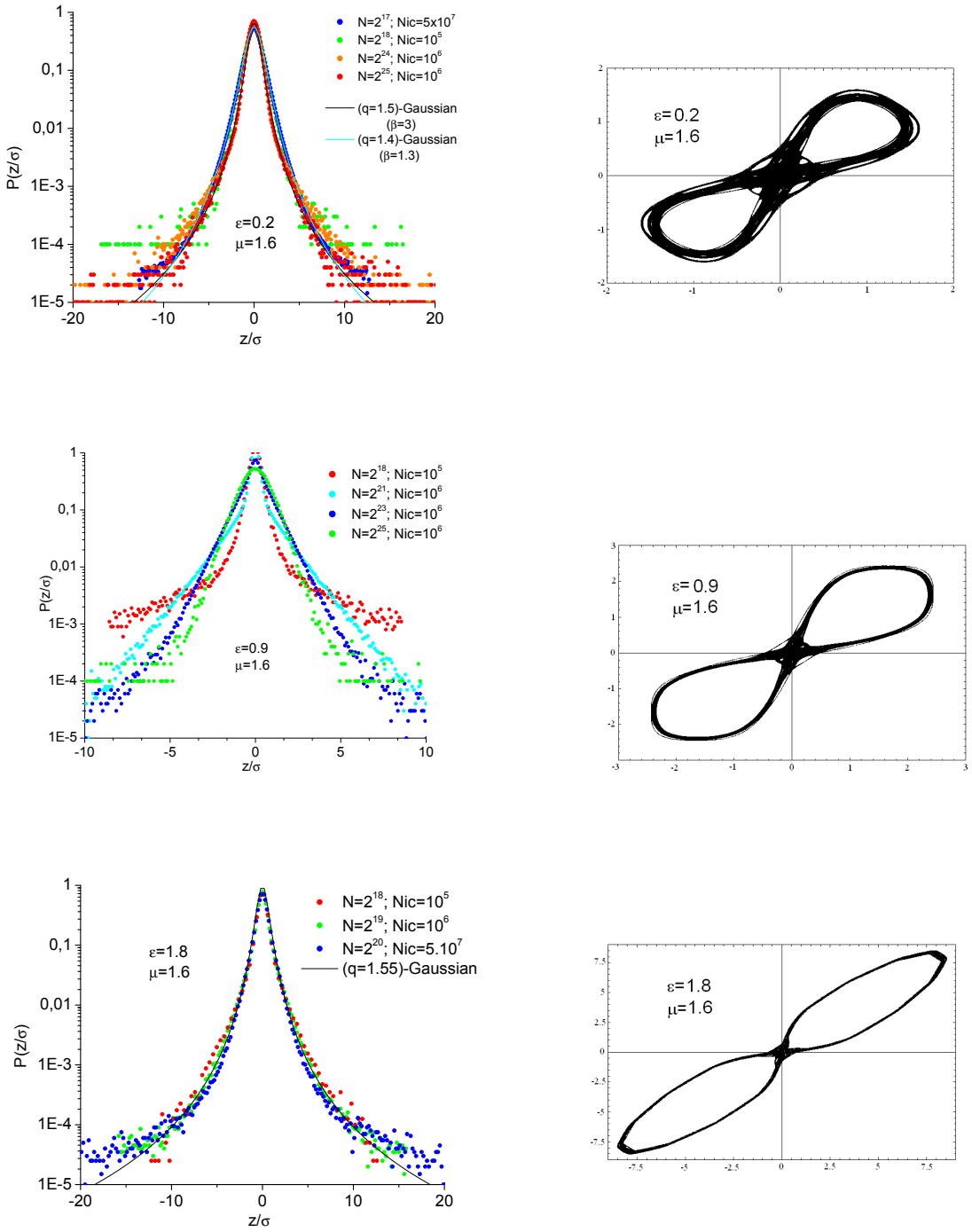

FIG. 3: Dynamical and statistical behavior of chaotic orbits of the MacMillan map for parameter values $\mu = 1.6$, and $\epsilon = 0.2, 0.9, 1.8$ (from top to bottom). The first column represents the pdfs of the normalized sums of iterates and the second depicts the corresponding phase space plot. N represents the number of (summed) iterates and N_{ic} is the number of initial conditions that have been randomly chosen from a square $(0, 10^{-6}) \times (0, 10^{-6})$.

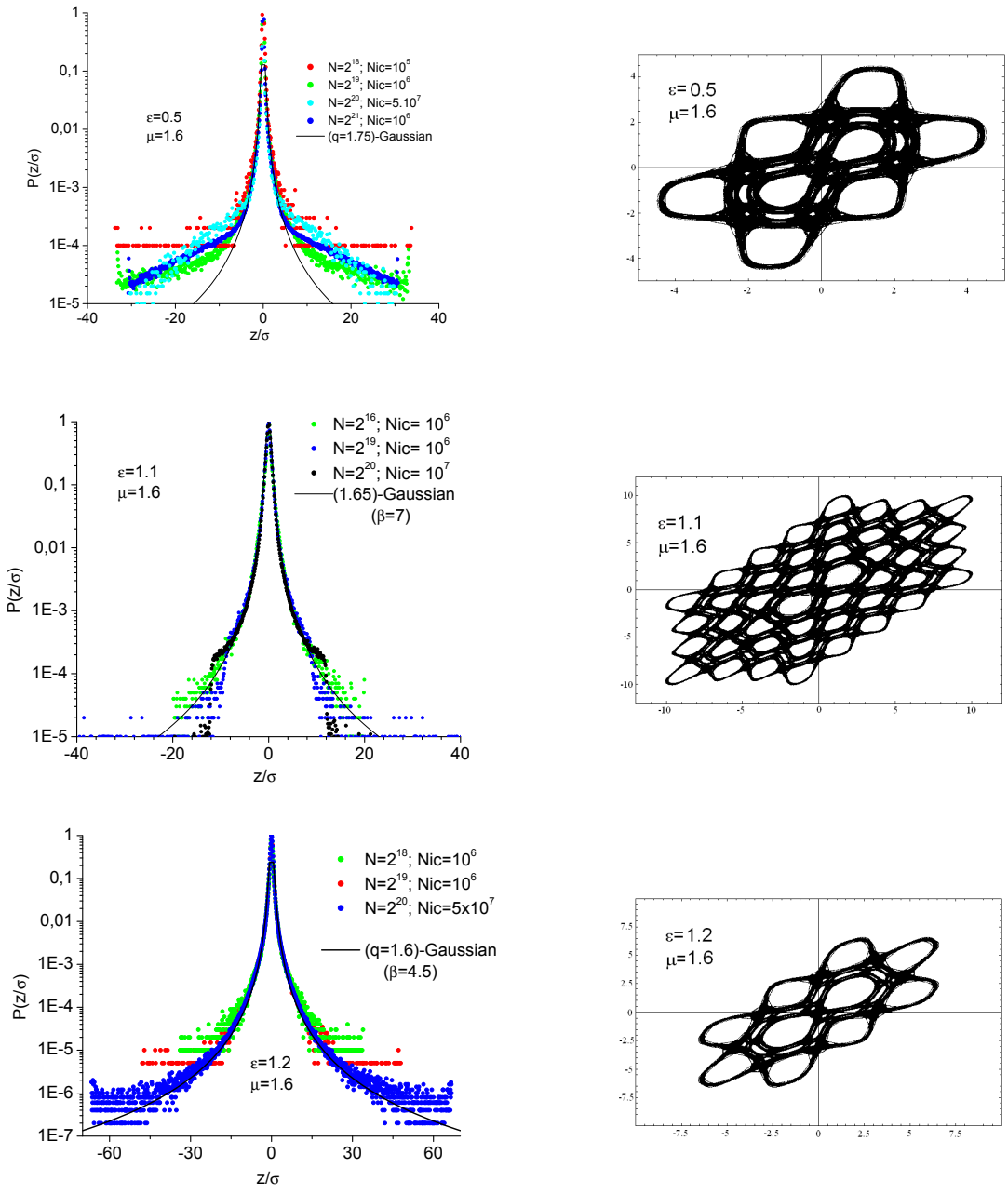

FIG. 4: Dynamical and statistical behavior of chaotic orbits of the MacMillan map for parameter values $\mu = 1.6$, and $\epsilon = 0.5, 1.1, 1.2$ (from top to bottom). The first column represents the pdfs of the normalized sums of iterates and the second depicts the corresponding phase space plot. N represents the number of (summed) iterates and N_{ic} is the number of initial conditions that have been randomly chosen from a square $(0, 10^{-6}) \times (0, 10^{-6})$.

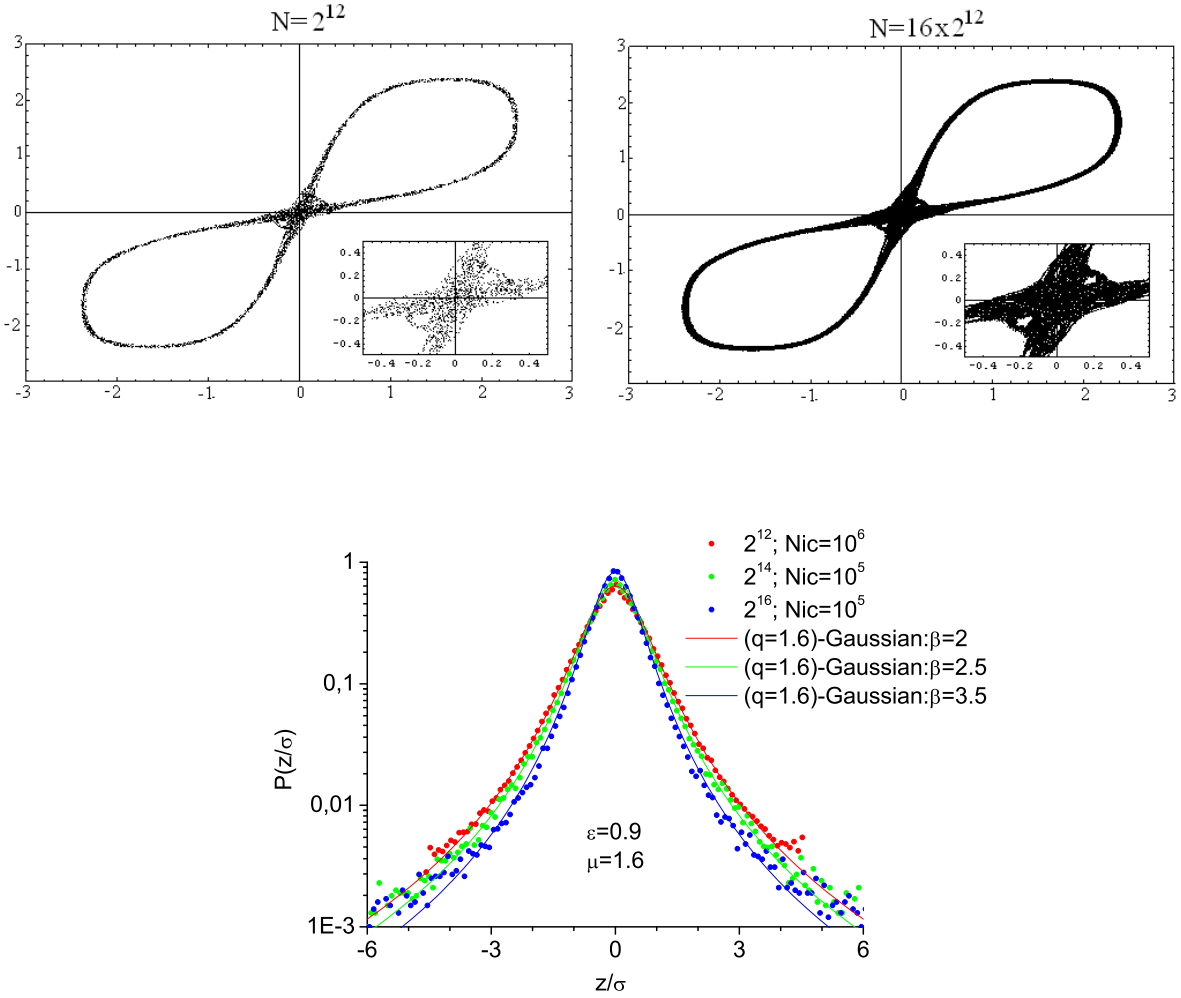

FIG. 5: ($\epsilon = 0.9$, $\mu = 1.6$)–MacMillan map phase space plots (first and second panel) and the corresponding PDFs (third panel) of the renormalized sums of iterates for $i = 1 \ldots N, N \leq 10^{16}$, starting from a randomly chosen initial condition in a square $(0, 10^{-6}) \times (0, 10^{-6})$.

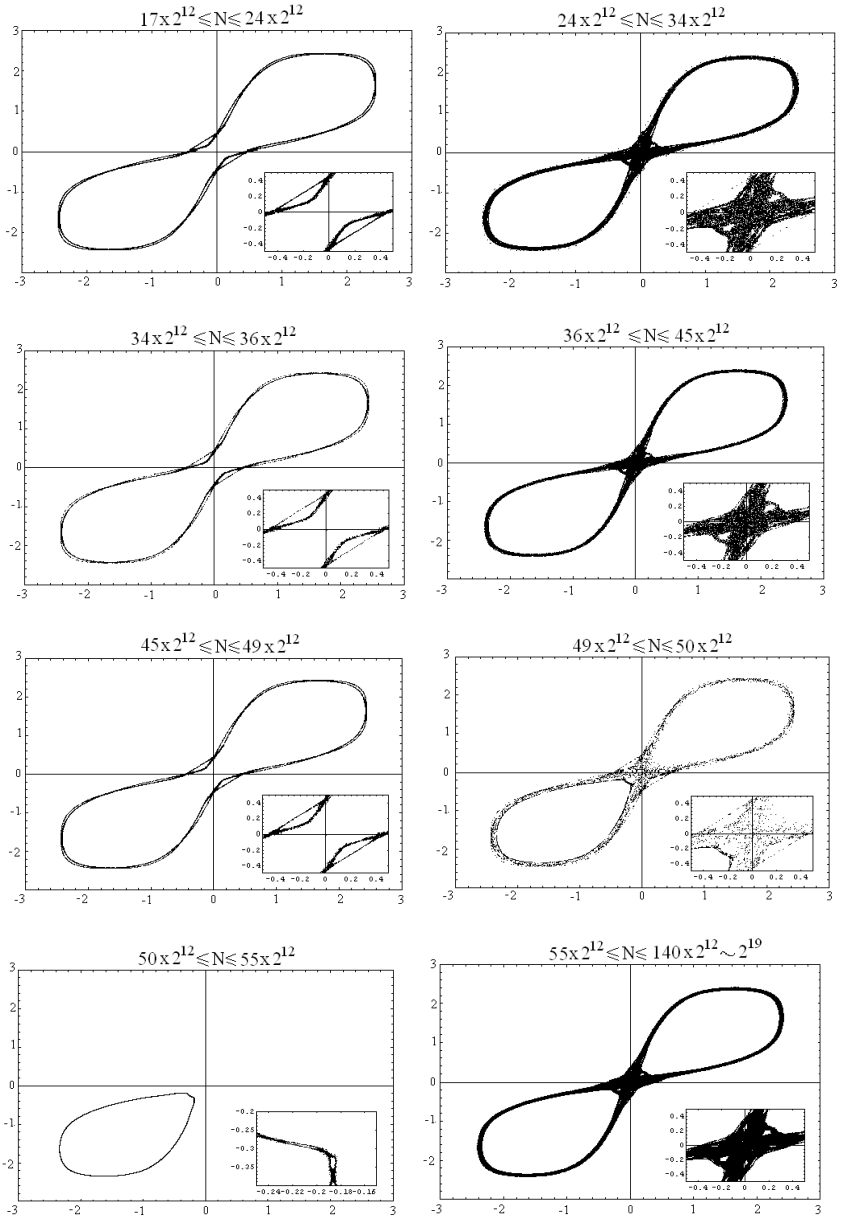

FIG. 6: ($\epsilon = 0.9$, $\mu = 1.6$)–MacMillan map partial phase space evolution. N iterates are calculated starting form a randomly chosen initial condition in a square $(0, 10^{-6}) \times (0, 10^{-6})$. N is the number of order of plotted iterates. Note the long-standing quasi-stationary states that sequentially superimpose on phase space plot.

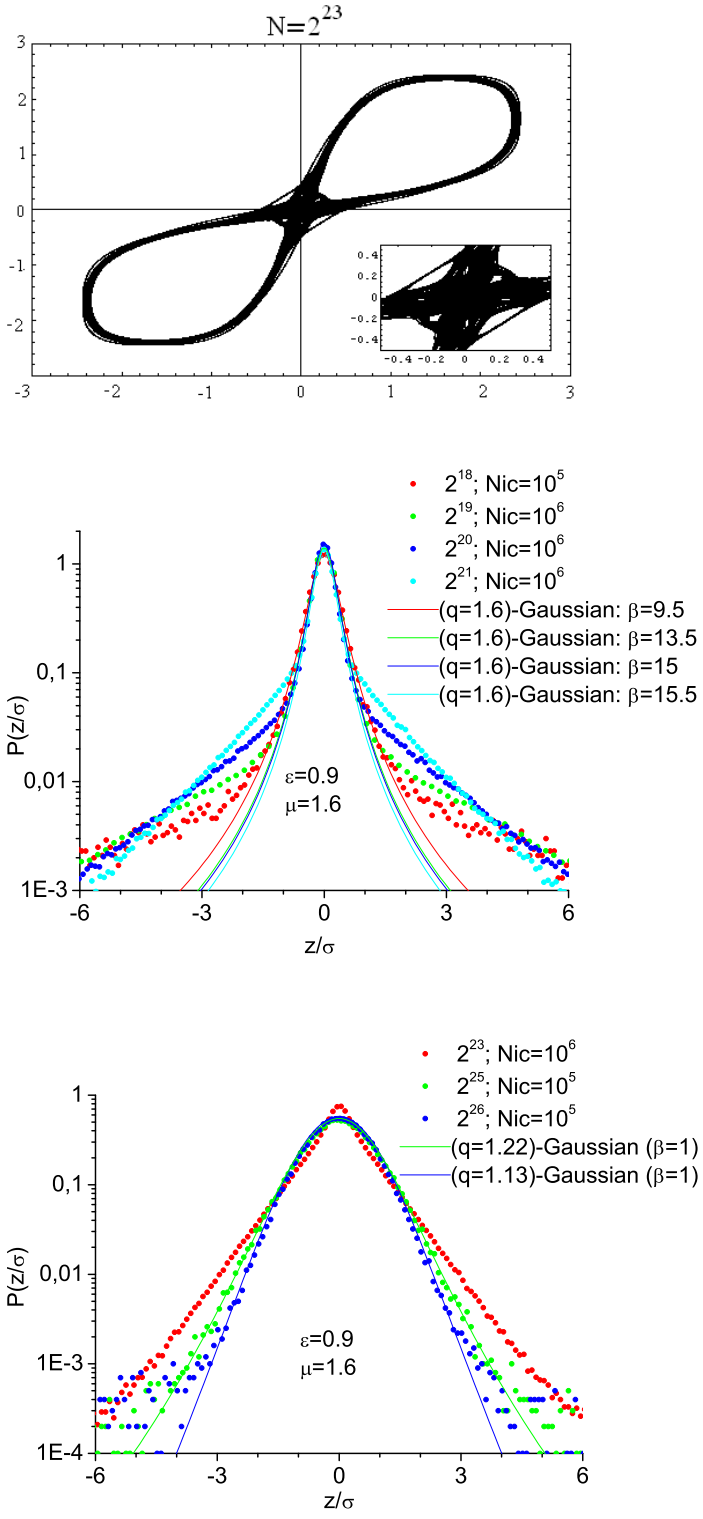

FIG. 7: ($\epsilon = 0.9$, $\mu = 1.6$)–MacMillan map phase space for $i = 1 \ldots N, N \geq 2^{23}$ plot iterates, starting form a randomly chosen initial condition in a square $(0, 10^{-6}) \times (0, 10^{-6})$. Corresponding PDFs.

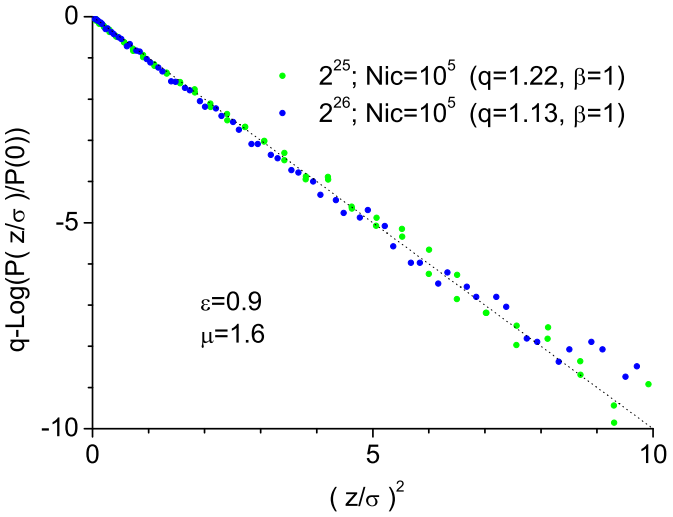

FIG. 8: Plots of the q–logarithm (inverse function of the q-exponential (**??**) vs. $(z/\sigma)^2$ applied to our data of the normalized pdf of the ($\epsilon = 0.9$, $\mu = 1.6$)–MacMillan map, for $N = 2^{25}$ and $N = 2^{26}$. For q–Gaussians this graph is a straight line, whose slope is $-\beta$) for the right value of q. Note also from these results that the pdfs approach a true Gaussian (with $\beta = 1$) since q tends to 1 as N increases.

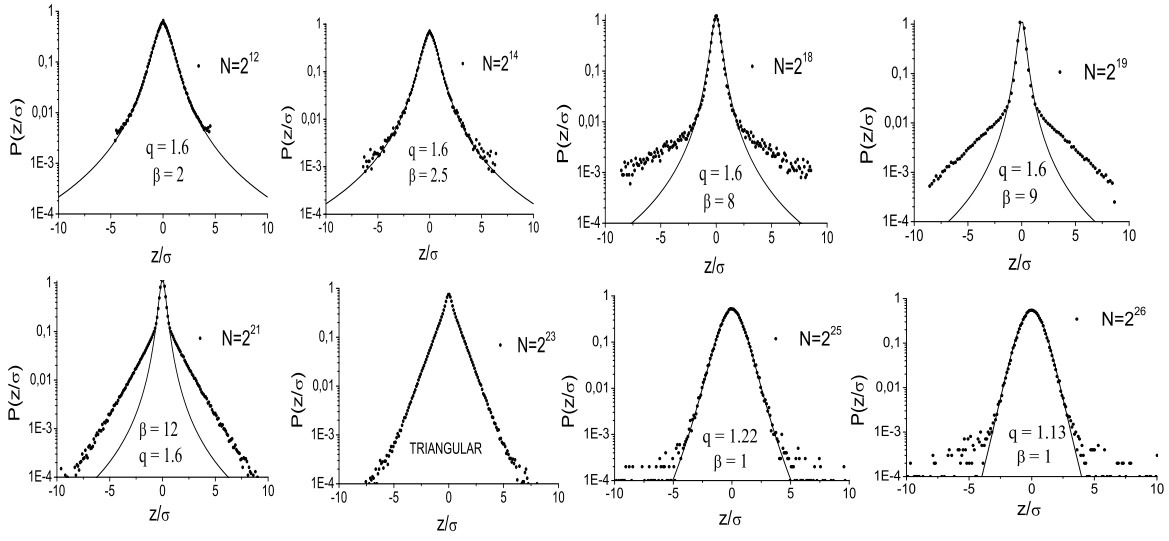

FIG. 9: Detailed evolution of the pdfs of the MacMillan map for $\epsilon = 0.9$, $\mu = 1.6$, as N increases from 2^{12} to 2^{26}.

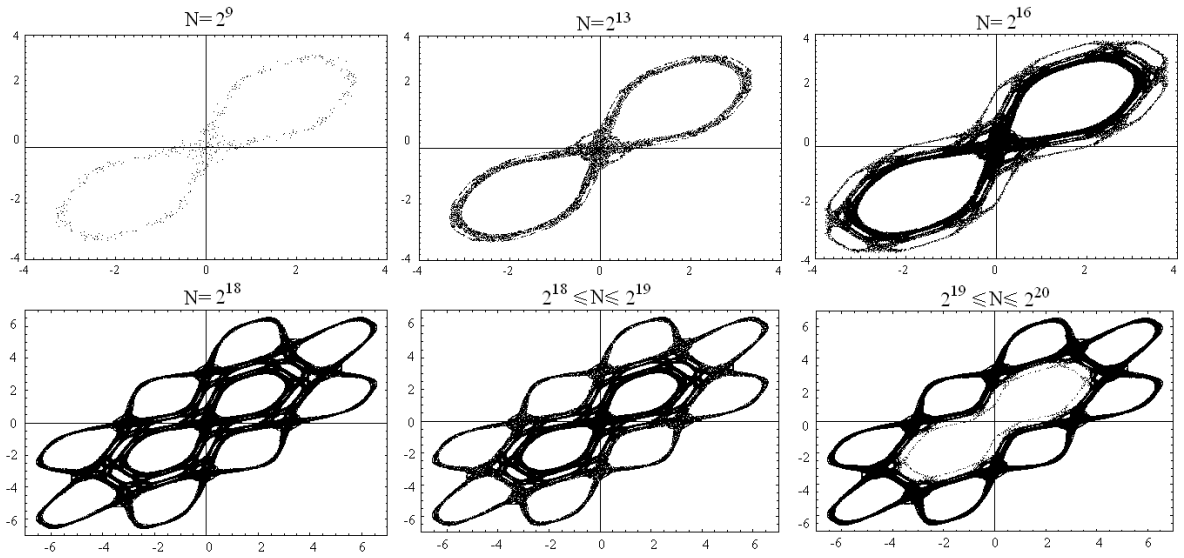

FIG. 10: Structure of phase space plot of the MacMillan map for parameter values $\epsilon = 1.2$ and $\mu = 1.6$, starting from a randomly chosen initial condition in a square $(0, 10^{-6}) \times (0, 10^{-6})$, and for $i = 1 \ldots N$ $(N = 2^{10}, 2^{13}, N^{16}, N^{18})$ iterates.

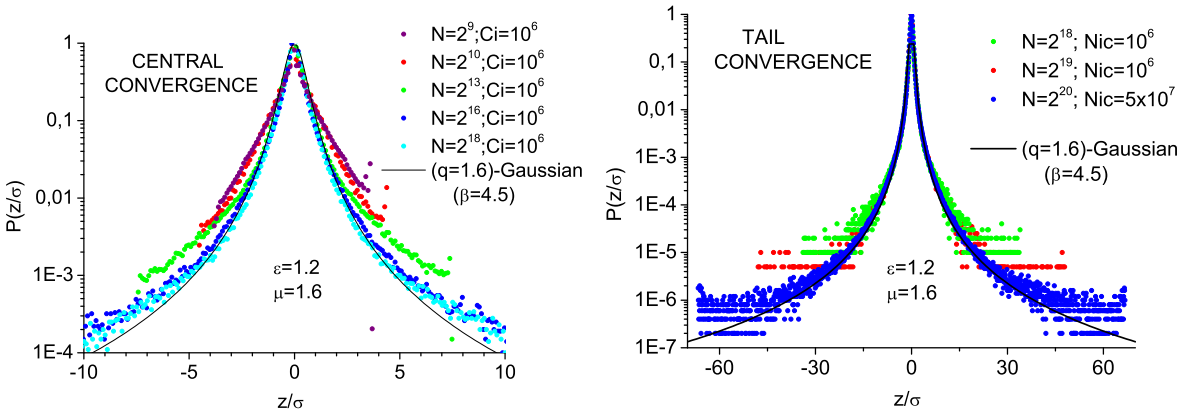

FIG. 11: Pdfs of the rescaled sums of iterates of the MacMillan map for $\epsilon = 1.2$ and $\mu = 1.6$ are seen here to converge to a $(q = 1.6)$-Gaussian. This is shown on the left panel for the central part of the pdf (for $N < 2^{18}$) and on the right panel for the tail part $(N > 2^{18})$.

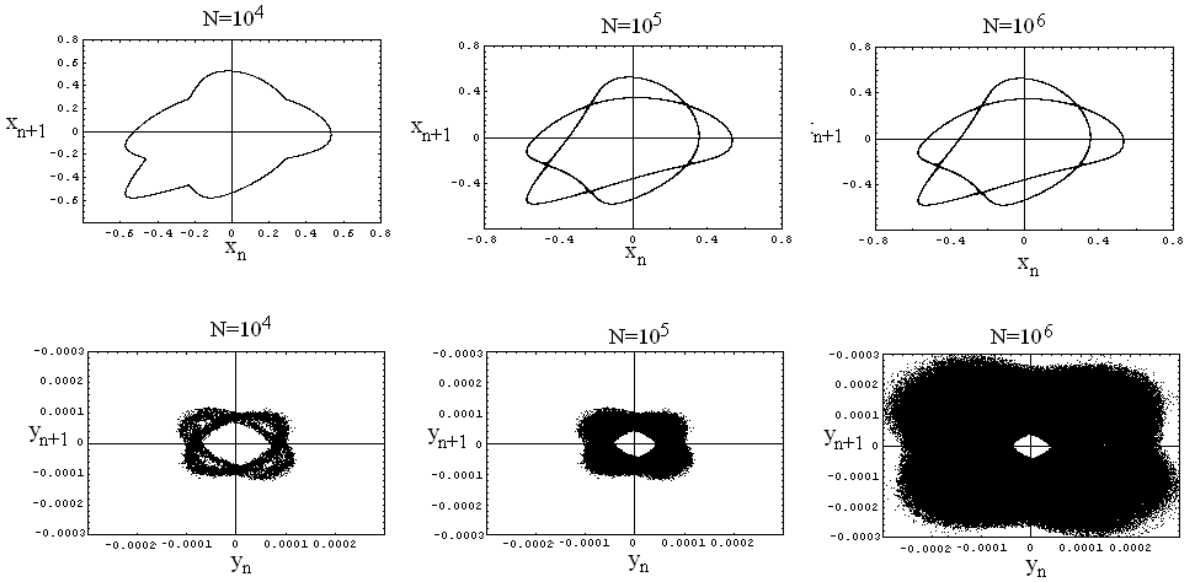

FIG. 12: The x_n, x_{n+1} (first row of panels) and y_n, y_{n+1} (second row of panels) projections of a chaotic orbit of (**??**), with $q_x = 0.21$, $q_y = 0.24$, $x_0 = -0.0049$ and initial conditions $x_1 = -0.5329$, $y_0 = 0.0001$ and $y_1 = 0$. N represents the number of plotted iterates.

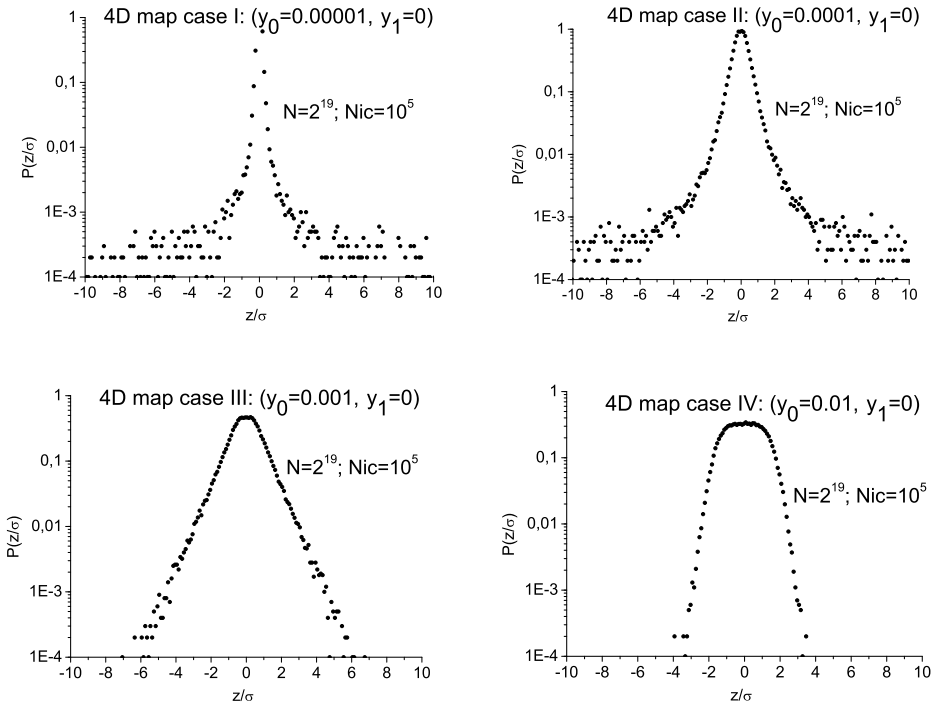

FIG. 13: Pdfs of the normalized sums of iterates of the y–chaotic orbit of the 4–dimensional map (**??**), for different y_0. In all cases, $q_x = 0.21$, $q_y = 0.24$, $x_0 = -0.0049$, $x_1 = -0.5329$, and $y_1 = 0$. N represents the number of (summed) iterates, N_{ic} is the number of randomly chosen initial conditions within an interval $[0.9y_0, y_0]$.

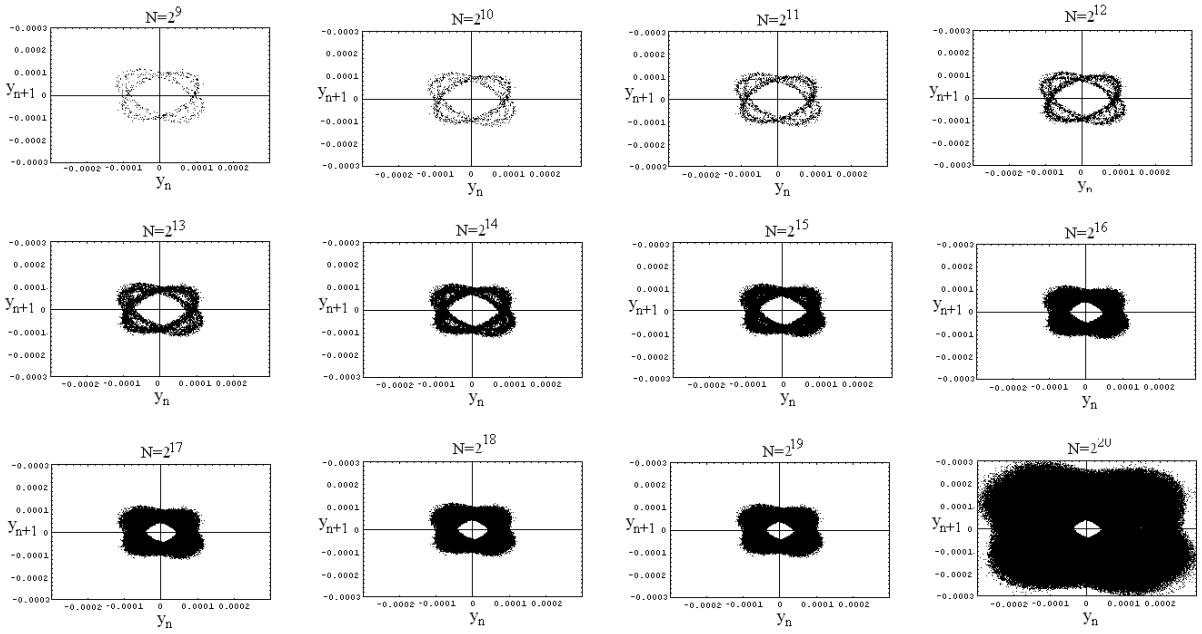

FIG. 14: Motion in the y_{n+1}, y_n plane for $q_x = 0.21$, $q_y = 0.24$ and initial conditions $x_0 = -0.0049$, $x_1 = -0.5329$, $y_0 = 0.0001$, $y_1 = 0$. N represents the number of iterates. Note the long–lived dynamical state with a maximum amplitude of about .0001 up to N^{19}, before the chaotic orbit expands to 3 times this amplitude at $N > 2^{20}$.

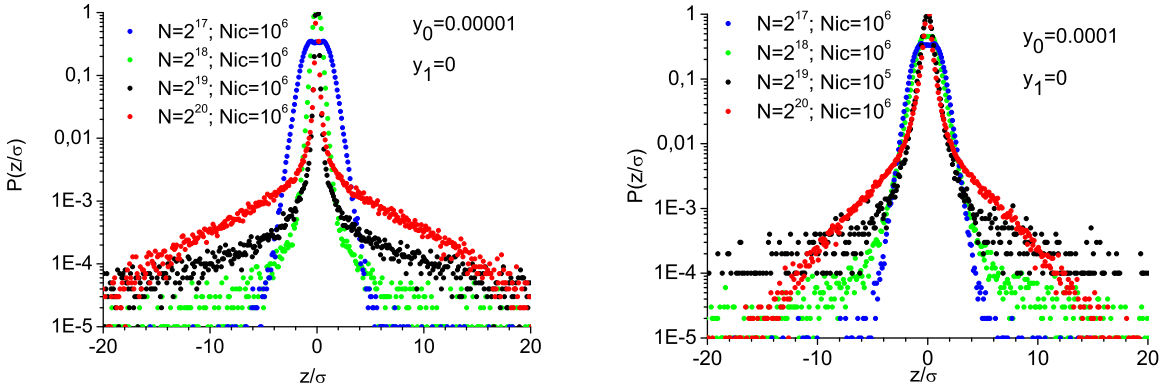

FIG. 15: Pdfs of the normalized sums of iterates of the y–chaotic orbit of the 4–dimensional map, for different initial conditions y_0 and numbers of (summed) iterates N. N_{ic} is the number of randomly chosen initial conditions from an interval $[0.9y_0, y_0]$. In all cases, $q_x = 0.21$, $q_y = 0.24$, $x_0 = -0.0049$, $x_1 = -0.5329$, and $y_1 = 0$.